PROCESS AND POST-PROCESSING OPTIMIZATION OF A HIGH-STRENGTH ALUMINUM MATRIX COMPOSITE FABRICATED BY LPBF

Marco Bona, Politecnico di Milano, Milano, Italy
Giovanni Agostoni, Leonardo S.p.a., Cascina costa, Italy
Gabriele Fantoni, Leonardo S.p.a., Cascina costa, Italy
Maurizio Tirelli, Leonardo S.p.a., Cascina costa, Italy
Grande Antonio Mattia, Politecnico di Milano, Milano, Italy

Abstract

Laser Powder Bed Fusion (LPBF) enables the production of complex aluminium components, but high-strength alloys like 2024 are prone to hot cracking. This work investigates the processability of a modified Al-Cu-Mg alloy containing titanium and ceramic grain refiners, which enhance printability and reduce defect formation. Laser power and scanning speed were varied under two different layer thickness configurations to assess their influence on density and mechanical performance. In both cases, relative densities above 99.5% were achieved. However, the low layer thickness condition led to superior mechanical properties, with a peak microhardness of 163.7 HV, compared to 154 HV for the high layer thickness. Post-processing heat treatments were applied to selected samples, including direct ageing and two solution plus artificial ageing routes. These thermal cycles enabled the development of different microstructures and resulted in improved mechanical performance in selected cases.

1. INTRODUCTION

Additive Manufacturing (AM), particularly Laser Powder Bed Fusion (LPBF), has revolutionized the production of complex metal components by enabling precise material deposition with minimal waste. This advancement is particularly relevant in the helicopter industry, where lightweight, high-strength materials are essential for improving performance, fuel efficiency, and payload capacity. The ability of AM to produce intricate geometries with optimized mechanical properties makes it an attractive solution for fabricating critical aluminium components, such as structural frames and dynamic drive system components, which must withstand operating conditions while minimizing weight. The most commonly used alloys in LPBF for aluminium components are Al-Si based systems, with AlSi10Mg being the most widely adopted. These alloys have been extensively studied in recent years and, although their performance can be improved through post-processing treatments, they are inherently unable to match the mechanical properties and high-performance requirements of advanced high-performance aluminium alloys [1] . However, the successful processing of high-strength aluminium alloys, such as those in the 2xxx, 6xxx, and 7xxx series, is significantly challenged by their susceptibility to hot cracking [2]. This issue arises due to the wide solidification temperature range and high thermal gradients, which lead to the formation of liquid films along grain boundaries and intergranular fractures upon cooling. A key factor in mitigating these defects is the careful selection and optimization of LPBF process parameters, including laser power, scanning speed, hatch spacing, and layer thickness. These parameters directly influence the thermal conditions during solidification, affecting melt pool stability, grain growth, and defect formation [3]. Improper parameter selection can exacerbate the formation of long dendrites, which trap residual liquid in interdendritic spaces. As solidification progresses, volume contraction and localized stresses can induce the separation of molten and solidified phases, resulting in crack formation. In addition to influencing solidification-related defects, process parameters also play a crucial role in determining the mechanical performance of the final component [4]. This is because they can affect the amount of alloying elements retained in solid solution, the resulting grain morphology, and the complex thermal history experienced by the material during the layer-by-layer melting and solidification process. To further suppress hot cracking and enhance processability, recent research has explored the addition of grain-refining inoculants such as titanium (Ti), zirconium (Zr), and scandium (Sc) [5]. These elements promote the formation of a fine equiaxed grain structure instead of columnar grains, which are particularly prone to crack formation due to their orientation and reduced ability to accommodate thermal stresses. The formation of cracks is especially prevalent in regions where a strong columnar structure dominates, and the transition to a more equiaxed microstructure is therefore a key objective in improving material integrity [6]. In particular, the formation of Al_3M (where M could be Ti, Zr, or Sc) particles at the melt pool boundaries refines the microstructure and improves the overall structural integrity of the material. Heat treatments are essential for improving the mechanical properties of aluminium alloys, primarily by controlling the amount and distribution of alloying elements in solid solution and in the form of strengthening precipitates [7]. However, components produced by LPBF exhibit a unique and complex thermal history, which often leads to inhomogeneous solute distributions and the formation of metastable phases [8], [9], complicating the post-processing phase. Solution heat treatments at elevated temperatures aim to dissolve alloying elements into the aluminium matrix, creating a supersaturated solid solution upon rapid cooling. This step helps reduce elemental segregation, relieve internal stresses, and prepare the material for aging treatments, where fine precipitates such as θ (Al_2Cu) and S (Al_2CuMg) form and strengthen the alloy by impeding dislocation motion through mechanisms like Orowan looping [10]. Despite these advantages, alloys that rely on age hardening at relatively low temperatures (typically 150–200 °C) present specific challenges. These temperatures are often too low to effectively relieve residual stresses generated during LPBF. Conversely, stress-relief (SR) treatments performed in the 300–400 °C range are more efficient in relaxing internal stresses but can cause undesirable effects, such as grain coarsening and partial dissolution of strengthening phases, ultimately compromising mechanical performance. If a solution treatment is applied afterward, there is a risk of further microstructural coarsening, which can erase the beneficial effects of the fine microstructure developed during rapid solidification. As a result, conventional heat treatment strategies are often unsuitable for LPBF-processed high-strength aluminium alloys, making the definition of an optimal thermal cycle particularly challenging.

This study investigates the interplay between LPBF process parameters and the resulting material properties, focusing on key factors such as density, microcrack formation, microstructure evolution, and mechanical performance. The material analysed is the high-strength aluminium alloy 2024 RAM2, a modified Al-Cu-Mg alloy incorporating Ti and ceramic reinforcements, as grain refiner, to improve printability and defect resistance. By systematically optimizing processing parameters and incorporating grain refiners, the study aims to identify conditions that enable defect-free manufacturing. Following this, different post-processing treatments were applied to evaluate how the complex microstructure can be further tailored to achieve the best possible performance, ensuring that LPBF-fabricated aluminium components meet the demanding requirements of helicopter applications.

2. MATERIALS AND METHODS

This study investigates the 2024 RAM2 aluminium alloy, a modified Al-Cu-Mg system incorporating titanium and ceramic particles to enhance microstructural refinement and suppress solidification-related defects. These additions act as effective nucleation agents, promoting grain refinement, reducing thermal stresses, and mitigating the formation of hot cracks. The manufacturing strategy was based on a systematic optimization of Laser Powder Bed Fusion (LPBF) parameters to enable the production of high-density, defect-minimized components. Specimens were fabricated by varying key process parameters—laser power (P_l), scan speed (v_{scan}), hatch distance (d_{hatch}), and layer thickness (t_{layer})—which collectively define the volumetric energy density (E_v), as expressed in Equation (1):

(1) $$E_v = \frac{P_l}{v_{scan} * d_{hatch} * t_{layer}}$$

In this study, laser power and scan speed were varied, and their values are presented in the paper as percentages normalized to the maximum tested value, which was set as 100%. The hatch distance was kept constant throughout all experiments. Two different layer thicknesses—referred to as low LT and high LT—were also tested to evaluate their influence on part quality.

To assess the impact of these parameters on material integrity, volumetric specimens were produced using various parameter combinations. The density of each sample was measured using a visual method: the specimens were polished to a mirror finish and analysed under optical microscopy. By adjusting the image contrast, internal voids appeared darker than the surrounding material and were quantified through image analysis. This allowed for the calculation of relative density based on the percentage of voids.

Once the optimal process parameters were identified, cubic specimens were fabricated to evaluate mechanical properties. Microstructural characterization was conducted using optical microscopy and scanning electron microscopy (SEM), which provided detailed views of grain morphology, phase distribution, and residual defects.

Mechanical performance was assessed through Vickers microhardness testing, performed using a 50 g load and a 15-second dwell time, specifically targeting the aluminium matrix. This testing enabled evaluation of both the influence of LPBF parameters and the effects of subsequent heat treatments.

Three post-processing heat treatment conditions were investigated: a T5 (direct ageing) treatment commonly used for AlSi10Mg alloys, and two T6 (solution treatment followed by artificial ageing) treatments. The first T6 condition followed a standard schedule typically used for cast 2024 alloys (T6-1), while the second was developed as a rapid industrial variant, aimed at reducing production time and costs by leveraging the fine LPBF microstructure (T6-2). The complete time-temperature profiles for each heat treatment step are detailed in Table 1.

Table 1: Heat treatment strategies.

Name	T_{sol}	t_{sol}	T_{age}	t_{age}
T5	-	-	180	20
T6-1	493	1.5	180	24
T6-2	493	1.5	150	12

3. PROCESS

3.1. Density

To systematically evaluate the influence of process parameters on part density, a total of 36 samples were fabricated using various combinations of laser power and scanning speed across the two distinct layer thickness configurations: low LT and high LT. These parameters were selected to span a broad range of E_v, allowing for the identification of optimal printing conditions. From the full set, a representative subset of 15 samples per layer thickness condition was selected for detailed density analysis. To obtain reliable and statistically meaningful data, 20 optical micrographs were captured for each specimen at 200× magnification. The samples were carefully polished to ensure flat and reflective surfaces, enabling accurate visual inspection of internal voids. Image analysis was performed by enhancing the contrast between the fully dense aluminium matrix and any internal porosity. Darker regions corresponding to pores were automatically segmented, and their area was quantified in relation to the total field of view. This method allowed the calculation of the relative density of each sample with high precision. The results are presented in Fig. 1, which shows the measured densities as a function of normalized volumetric energy density. For the low LT condition (Figure 1a), a clear and consistent trend was observed: once the energy density exceeded approximately 50% of the maximum tested value, most samples reached a density plateau, with relative densities commonly exceeding 99.5%. Within this regime, a stable processing window was identified between 54% and 75% of the maximum E_v, which is highlighted in green in the figure. This region represents an optimal balance between sufficient melting and avoidance of excessive thermal input. In contrast, the behaviour of samples produced using the high LT configuration (Figure 1b) was more variable. Although no well-defined plateau was observed, a relatively narrow processing window between 65% and 82% of the maximum energy density showed the best overall results, with several samples again achieving densities above 99.5%. Despite the broader scatter in this case, this range is considered the most favourable for producing dense parts under high LT conditions. Importantly, samples produced at the highest energy densities, especially in the low LT group, were excluded from the optimal range, despite sometimes showing high density values. These conditions were associated with several detrimental effects. Very high energy inputs can lead

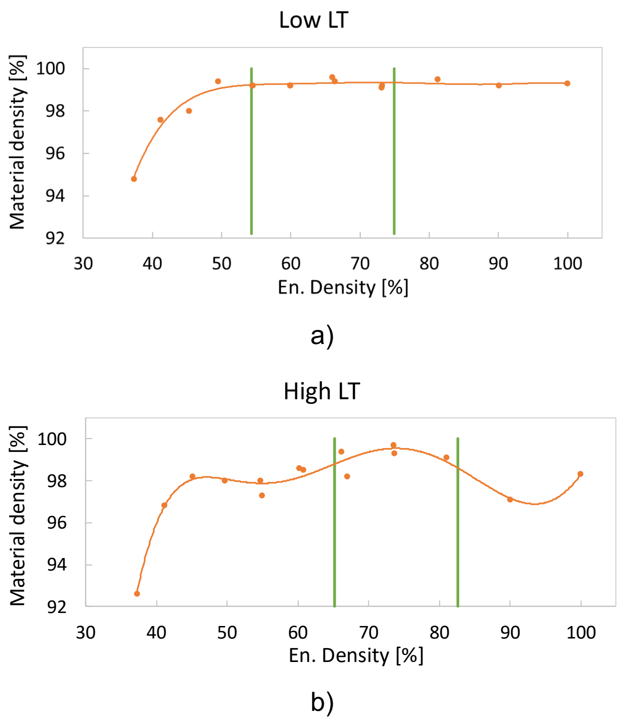

Figure 1: Relative density vs. E_v for samples with (a) low layer thickness and (b) high layer thickness.

to keyhole porosity, due to deep and unstable melt pools that trap gas during solidification [11]. Additionally, high temperatures can cause selective evaporation of alloying elements, particularly magnesium (Mg), which is highly volatile. The loss of Mg compromises the alloy's capacity to form strengthening precipitates, ultimately reducing mechanical performance. Excessive energy also promotes melt pool instability, increasing the likelihood of spattering, surface roughness, and thermal fluctuations during solidification. Finally, high energy densities tend to favour the formation of columnar grains over equiaxed ones, resulting in a more anisotropic and less desirable microstructure [12]. For these reasons, even though some samples produced under these conditions exhibited high relative densities, they were not considered viable and were excluded from the optimal processing window. The optimal range is highlighted in Figures 1a and 1b, delineated by green lines.

3.2. **Hardness**

To further investigate the relationship between process parameters and mechanical performance, all samples that fell within the optimal density window, identified in the previous section, were selected for microhardness testing. This subset included 13 samples produced with low LT and 9 samples fabricated with high LT, reflecting the parameter combinations that resulted in the highest relative densities. Each of these samples underwent Vickers microhardness testing, with six measurements per specimen taken on the aluminium matrix to ensure statistical

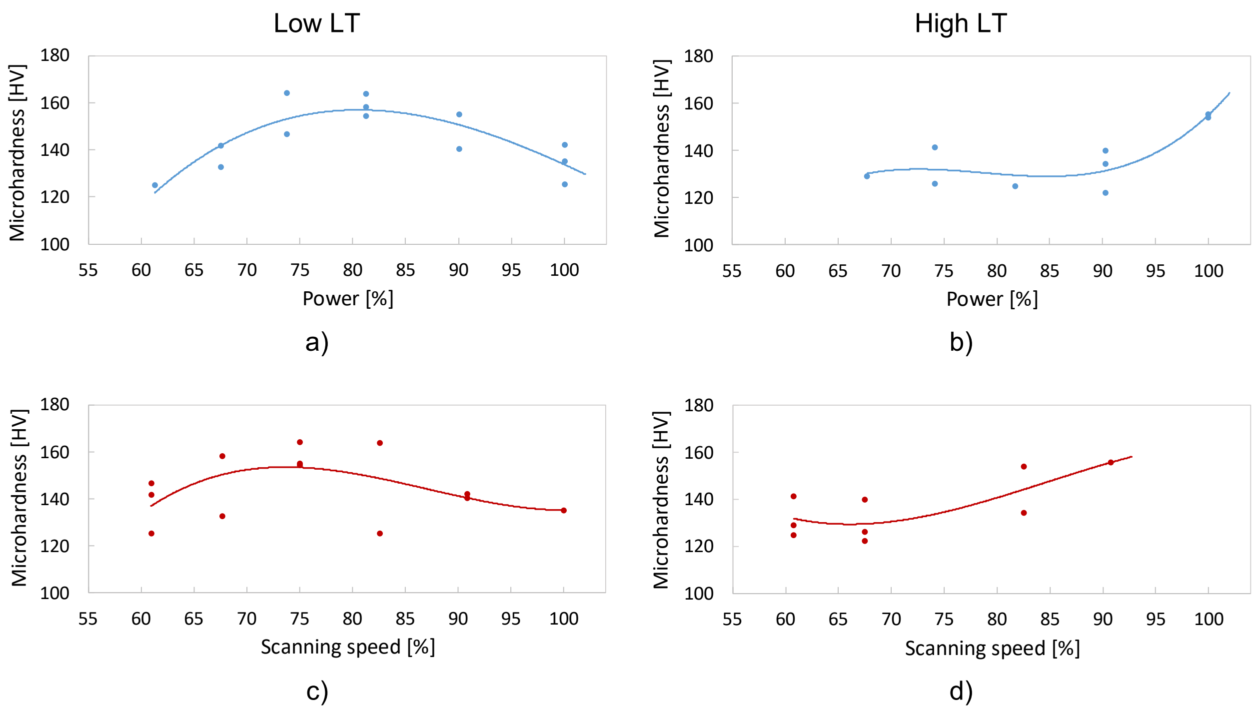

Figure 2: Microhardness vs. (a) laser power and (c) scanning speed for samples with low layer thickness; (b) laser power and (d) scanning speed for samples with high layer thickness.

reliability. The aim was to correlate microhardness values with laser power and scanning speed, and to identify any trends associated with the variation in energy input across both thickness batches. The results for the low LT group are reported in Fig. 2a and 2c, showing microhardness values plotted against E_v and v_{scan}. A clear peak in mechanical performance is observed, with the highest values occurring in the region of approximately 81% of maximum laser power and 75% of maximum scanning speed. Within this area, the best-performing sample exhibited a microhardness of 163.7 HV. For samples produced using the high LT configuration, the results are presented in Fig. 2b and 2d. While these specimens also reached relatively high hardness values (up to 154 HV), the trend differs from that seen in the low LT group. In this case, a continuous increase in hardness was noted with rising power and scan speed, and no clear plateau was reached within the tested parameter range. This suggests that the optimal mechanical performance for high LT may lie beyond the upper bounds of laser power and scanning speed evaluated in this study. However, further investigation was not possible due to limitations in the maximum laser power output of the LPBF machine. Taking into account the more stable densification behaviour, the superior microhardness values, and the reduced surface roughness associated with thinner layers—which is particularly beneficial for enhancing fatigue resistance—the low LT configuration was selected for further material characterization. Several cubic specimens were fabricated using the specific combination of laser power and scanning speed that corresponded to the observed peak in mechanical properties. These samples served as the basis for subsequent microstructural analysis and heat treatment studies aimed at fully assessing the performance potential of the optimized LPBF-processed alloy.

3.3. Microstructure

The as-built microstructure of the 2024 RAM2 alloy, shown in Fig. 3a, exhibits the typical characteristics of components produced by laser-based technologies. The melt pool boundaries are clearly defined, and no significant porosity or hot cracking is observed, indicating stable processing conditions. Optical and scanning electron microscopy reveal a homogeneous and ultra-fine equiaxed grain structure, with average grain sizes on the order of 1 µm. This fine structure results from the rapid solidification rates typical of LPBF and the presence of titanium and ceramic particles, which do not fully melt during processing. These particles serve as heterogeneous nucleation sites, effectively promoting grain refinement and helping to reduce thermal stresses during solidification. The reinforcing phases are clearly distinguishable from the aluminium matrix: titanium particles appear larger and nearly spherical (around 20 µm in diameter), while the ceramic phase is finer, darker, and irregular in shape, typically between 1 and 5 µm. Along grain boundaries, a continuous eutectic network is observed, enriched with copper and magnesium, which segregate during solidification. These microstructural features—ultra-fine grains, refined eutectic regions, and solid solution strengthening—contribute to the excellent mechanical properties observed in the as-built condition. The absence of defects and the high level of microstructural refinement confirm the effectiveness of both the alloy design and the LPBF parameters in producing high-performance, structurally sound components. These observations are consistent with findings reported in previous studies on the same material system [13], [14].

4. POST-PROCESS

4.1. Microstructure

Moving on to the analysis of the heat-treated microstructures, the specimen subjected to the T5 condition—direct aging at 180 °C for 20 hours—maintains the ultra-fine equiaxed grain structure characteristic of the as-built state (Fig. 3b). The eutectic network remains visible along the grain boundaries, suggesting that it has not dissolved at this relatively low temperature. However, compared to the as-built condition, the grain contours appear slightly less defined. This is likely due to the formation of early-stage precipitates within the grains. These observations are in line with the expected effects of a low-temperature aging treatment, where diffusion is limited to short-range atomic movement. As such, precipitation occurs without triggering recrystallization or significant grain growth, preserving the original microstructure while initiating the strengthening process through solute clustering. In contrast, the microstructures of the specimens aged under T6 (Fig. 3c and 3d) conditions appear substantially different and largely similar to each other. The eutectic network has disappeared, indicating its dissolution during the high-temperature solution treatment phase. Instead, a high density of nanometric precipitates is observed throughout the matrix. Given the aging temperatures used in both

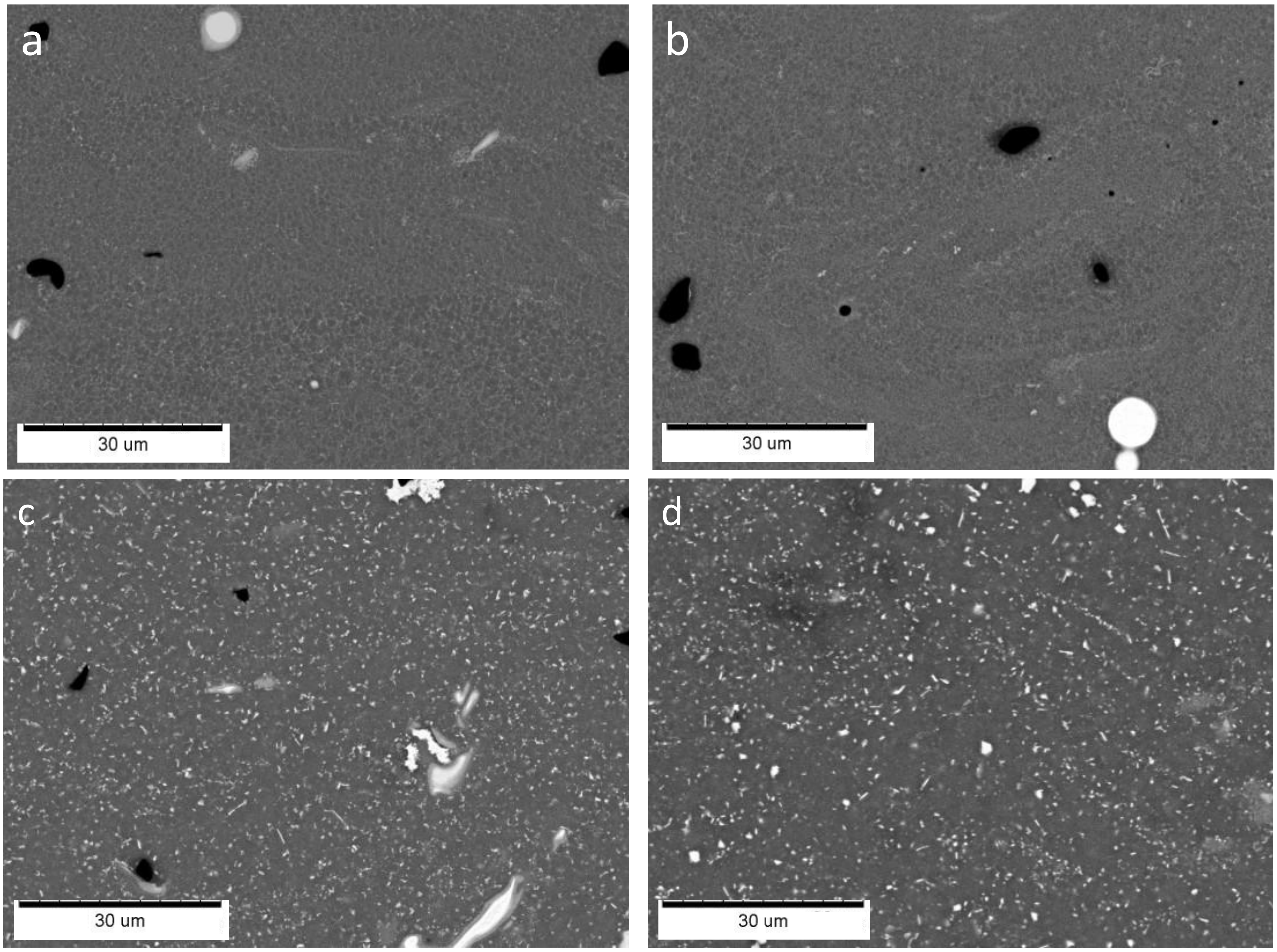

Figure 3: SEM images at 2000× of samples in different conditions: (a) as-built, (b) aged at 180 °C for 20 h, (c) T6 with ageing at 180 °C for 24 h, and (d) T6 with ageing at 150 °C for 12 h.

treatments, these precipitates are likely associated with the S-phase (Al_2CuMg), which is known to provide the most effective mechanical strengthening in this alloy system. No evidence of coarsening of second phases is visible, confirming that the selected time-temperature combinations are effective in promoting precipitation without leading to over-aging. These microstructural features are expected to enhance mechanical performance significantly, especially in terms of hardness and strength, due to the uniform and fine distribution of strengthening phases.

4.2. Mechanical performance

The microhardness values corresponding to each thermal condition are summarised in Table 2. The as-built samples—fabricated using the optimal LPBF parameters at low layer thickness—exhibited an average hardness of 163.7 ± 11.4 HV. This relatively high initial value reflects the contribution of the ultra-fine grain structure and the high solute supersaturation characteristic of rapid solidification. However, the elevated standard deviation suggests microstructural metastability, potentially associated with residual stresses, local segregation, and early-stage precipitation phenomena. Following direct ageing at 180 °C for 20 hours (T5 condition), the average microhardness was 157.9 ± 6.6 HV. While this value remains within the uncertainty range of the as-built condition and thus does not indicate a statistically significant change, the lower standard deviation points to increased microstructural stability. This behaviour is consistent with the limited atomic mobility at this temperature, which allows for initial precipitation and relaxation without significantly modifying the grain morphology or eliminating the eutectic network. The two T6 treatments, both involving solution annealing at 493 °C for 1.5 hours followed by artificial ageing, produced distinct results. The conventional T6 treatment—artificial ageing at 180 °C for 24 hours—resulted in a microhardness of 171.1 ± 4.6 HV. The increase in hardness reflects the formation of fine, uniformly distributed S-phase precipitates, which effectively obstruct dislocation motion. The comparatively low standard deviation suggests a stable and fully developed precipitation state, likely indicating that the system has reached or slightly surpassed the peak ageing condition. In contrast, the rapid T6 cycle—featuring artificial ageing at 150 °C for 12 hours—yielded the highest hardness value of 204.3 ± 9.6 HV. This significant increase (~24% over the as-built condition) can be attributed to the formation of a denser and more refined precipitate population, which provides enhanced resistance to plastic deformation. The higher standard deviation, however, implies increased heterogeneity, possibly due to incomplete transformation or spatial variations in the ageing response. This suggests that the peak ageing condition may not yet have been fully achieved under these parameters. In summary, while both T6 treatments enhance the alloy's mechanical response, the conventional strategy (T6-1) yields a more stable condition with modest improvement, whereas the rapid T6 offers superior strengthening at the cost of slightly increased variability (T6-2). These results highlight the potential of accelerated heat treatment protocols to improve performance and reduce production times for LPBF-manufactured aluminium components.

Table 2: Vickers microhardness results for the alloy in different heat treatment conditions.

Heat treatment	HV	Dev std
AB	163.7	± 11.4
T5	157.9	± 6.6
T6-1	171.1	± 4.6
T6-2	204.3	± 9.6

5. CONCLUSIONS

This study investigated the influence of LPBF processing parameters on the microstructural and mechanical properties of the high-strength aluminium alloy 2024 RAM2, a modified Al-Cu-Mg alloy reinforced with Ti and ceramic particles to enhance processability and reduce defect formation. The primary objective was to identify optimal process conditions that enable defect-free additive manufacturing of an alloy traditionally considered non-printable, and to evaluate the effect of post-processing strategies on the resulting performance, with a view toward applications in the aerospace sector.

The experimental results demonstrated that, through the combined use of in-situ grain refiners and parameter optimization, it was possible to fabricate samples with relative densities exceeding 99.5%. In particular, the use of thinner layer thicknesses resulted in more consistent densification behaviour, with density reaching a plateau within a specific window of volumetric energy density. In contrast, samples produced with thicker layers exhibited more variable densification, without a clearly defined plateau, indicating reduced process stability under these conditions.

Microhardness measurements further supported these trends. Samples produced with thinner layers not only reached peak hardness values within the optimal densification window but also exhibited higher absolute hardness compared to their thick-layer counterparts. These findings, along with the superior surface quality achievable with thinner layers—which is especially relevant for fatigue-critical components—led to the selection of low-layer-thickness samples for further post-processing investigations.

A range of heat treatments commonly employed for AM AlSi10Mg alloys and cast 2024 alloys were applied to the as-built samples. While all post-processing strategies resulted in improved mechanical properties relative to the as-built condition, the most effective approach was a modified T6 treatment specifically developed in this study. This cycle, involving solution treatment followed by a shorter and lower-temperature artificial ageing step, produced the highest hardness values among all tested conditions. Moreover, it offers potential advantages in terms of processing efficiency, enabling shorter cycle times and lower energy consumption, which are critical factors for the industrial scalability of LPBF-produced components.

Overall, the results confirm that the 2024 RAM2 alloy, when processed under optimized LPBF conditions and appropriately post-treated, can meet the performance requirements necessary for demanding structural applications, such as those in the aerospace and helicopter sectors.

6. FUTURE DEVELOPMENTS

The 2024 RAM2 alloy has shown excellent mechanical performance, making it a strong candidate for aerospace and rotorcraft applications. Its refined microstructure and high strength confirm the material's potential in demanding structural environments.

However, its complexity introduces challenges that must be addressed before large industrial adoption.

This study highlights how sensitive the material is to process variations and the need for well-defined, repeatable workflows.
To fully understand the potential and limitations of 2024 RAM2, it will be important to compare it with other advanced aluminium alloys using similar grain refinement approaches.

Author contact:

Marco Bona: marco.bona@polimi.it
Giovanni Agostoni: giovanni.agostoni@leonardo.com.
Gabriele Fantoni: gabriele.fantoni@leonardo.com
Maurizio Tirelli: maurizio.tirelli@leonardo.com
Antonio Mattia Grande: antonio-mattia.grande@polimi.it

7. ACKNOWLEDGMENTS

This work was supported by the Italian National Recovery and Resilience Plan (PNRR), within the framework of the project identified by CUP D43C23002190008.
The authors would also like to express their sincere gratitude to Ph.D. Tiziana Biasutti for her valuable assistance and support throughout the development of this study.

8. REFERENCES

[1] K. Riener, T. Pfalz, F. Funcke, and G. Leichtfried, 'Processability of high-strength aluminum 6182 series alloy via laser powder bed fusion (LPBF)', *International Journal of Advanced Manufacturing Technology*, vol. 119, no. 7–8, pp. 4963–4977, Apr. 2022, doi: 10.1007/s00170-022-08673-8.

[2] I. M. Kusoglu, B. Gökce, and S. Barcikowski, 'Research trends in laser powder bed fusion of Al alloys within the last decade', Dec. 01, 2020, *Elsevier B.V.* doi: 10.1016/j.addma.2020.101489.

[3] J. L. Leirmo, 'High Strength Aluminium Alloys in Laser-Based Powder Bed Fusion - A Review', in *Procedia CIRP*, Elsevier B.V., 2021, pp. 1747–1752. doi: 10.1016/j.procir.2021.11.294.

[4] W. Stopyra, K. Gruber, I. Smolina, T. Kurzynowski, and B. Kuźnicka, 'Laser powder bed fusion of AA7075 alloy: Influence of process parameters on porosity and hot cracking', *Addit Manuf*, vol. 35, Oct. 2020, doi: 10.1016/j.addma.2020.101270.

[5] J. R. Croteau *et al.*, 'Microstructure and mechanical properties of Al-Mg-Zr alloys processed by selective laser melting', *Acta Mater*, vol. 153, pp. 35–44, Jul. 2018, doi: 10.1016/j.actamat.2018.04.053.

[6] Y. Wang *et al.*, 'Laser powder bed fusion of Zr-modified Al–Cu–Mg alloy: Crack-inhibiting, grain refinement, and mechanical properties', *Materials Science and Engineering: A*, vol. 838, Mar. 2022, doi: 10.1016/j.msea.2022.142618.

[7] M. Laleh *et al.*, 'Heat treatment for metal additive manufacturing', Mar. 01, 2023, *Elsevier Ltd*. doi: 10.1016/j.pmatsci.2022.101051.

[8] J. Fiocchi, C. A. Biffi, C. Colombo, L. M. Vergani, and A. Tuissi, 'Ad Hoc Heat Treatments for Selective Laser Melted Alsi10mg Alloy Aimed at Stress-Relieving and Enhancing Mechanical Performances', *JOM*, vol. 72, no. 3, pp. 1118–1127, Mar. 2020, doi: 10.1007/s11837-019-03973-z.

[9] S. Cacace, A. Gökhan Demir, G. Sala, and A. Mattia Grande, 'Influence of production batch related parameters on static and fatigue resistance of LPBF produced AlSi7Mg0.6', *Int J Fatigue*, vol. 165, Dec. 2022, doi: 10.1016/j.ijfatigue.2022.107227.

[10] C. Senthamarai Kannan, S. Sai Sree Chandra, G. Punith Krishnan, and S. Pravin Raj, 'A review on additive manufacturing of AA2024

and AA6061 alloys using powder bed fusion', in *IOP Conference Series: Materials Science and Engineering*, IOP Publishing Ltd, Dec. 2020. doi: 10.1088/1757-899X/988/1/012002.

[11] A. Samaei *et al.*, 'Benchmark study of melt pool and keyhole dynamics, laser absorptance, and porosity in additive manufacturing of Ti-6Al-4V', *Progress in Additive Manufacturing*, Jan. 2024, doi: 10.1007/s40964-024-00637-6.

[12] M. Abdi, S. Mosbah, and M. Ayadi, 'High fidelity multi-physics modeling of laser metal interaction and keyhole dynamics in powder bed fusion', *Progress in Additive Manufacturing*, Feb. 2024, doi: 10.1007/s40964-024-00702-0.

[13] M. Bona and A. M. Grande, 'Optimization of Post-Processing Heat Treatment for an High-Performance Aerospace Grade Aluminum Alloy Manufactured by Laser Powder Bed Fusion (LPBF)', in *AIAA SCITECH 2025 Forum*, Reston, Virginia: American Institute of Aeronautics and Astronautics, Jan. 2025. doi: 10.2514/6.2025-1552.

[14] M. Bona and A. M. Grande, 'OPTIMIZATION OF POST-PROCESSING HEAT TREATMENT FOR LPBF MODIFIED 2024 ALUMINIUM ALLOY', in *ICAS proceedings*, Florence, Sep. 2024. Accessed: Feb. 28, 2025. [Online]. Available: https://re.public.polimi.it/bitstream/11311/1275141/1/BONAM01-24.pdf